ACS OMEGA

Open Access

http://pubs.acs.org/journal/acsodf

Article

The Preparation and Characterization of Electrospun Chitosan-Gelatin Nanofibers Containing Copper−Metal−Organic Frameworks Loaded with Curcumin and Chrysin as Antibacterial Wound Dressings

Soo Ghee Yeoh,* Yun Khoon Liew, Wei Meng Lim, Norizah Abdul Rahman, and Yoon Yee Then*

Cite This: *ACS Omega* 2025, 10, 21065−21076

Read Online

ACCESS | Metrics & More | Article Recommendations | Supporting Information

ABSTRACT: An electrospun chitosan-gelatin (CS-GL) nanofiber encapsulated with the curcumin (CUR)-chrysin (CHR)-loaded copper (Cu) metal−organic framework (MOF) was successfully synthesized in this study. A high percentage of encapsulation efficiency (99.2%) of CUR and CHR in Cu-MOF-CUR-CHR was yielded. Other than the confirmation of the successful fusion of MOFs with CUR-CHR in CS-GL/Cu-MOF-CUR-CHR nanofibers using Fourier-transform infrared (FTIR) spectroscopy, the scanning electron microscopy (SEM) images depicted an average diameter in the range of 302−380 nm. The percentage of cumulative drug release of CS-GL/20% Cu-MOF-CUR-CHR nanofibers in phosphate-buffered solution at pH 7.4 after 48 h was 98.9%, which was higher than CS-GL/CUR-CHR nanofibers without Cu-MOFs. In the cytotoxicity test on Human epidermal keratinocytes cell line cells, it was noticed that 1% and 5% CS-GL/Cu-MOF-CUR-CHR nanofibers exhibited high cell survival (>90%). Through the colony counting method, the logarithm reduction values (LRVs) of CS-GL/5% Cu-MOF-CUR-CHR nanofibers were 2.69 against *Staphylococcus aureus* and 1.87 against *Pseudomonas aeruginosa*. It was noteworthy that the CS-GL/Cu-MOF-CUR-CHR nanofiber exhibited a higher antibacterial activity against Gram-positive than Gram-negative bacteria. Overall, the biocompatible CS-GL/Cu-MOF-CUR-CHR nanofibers with an effective antibacterial effect have the potential to be used as an alternative to antibiotics in antibacterial wound dressing applications.

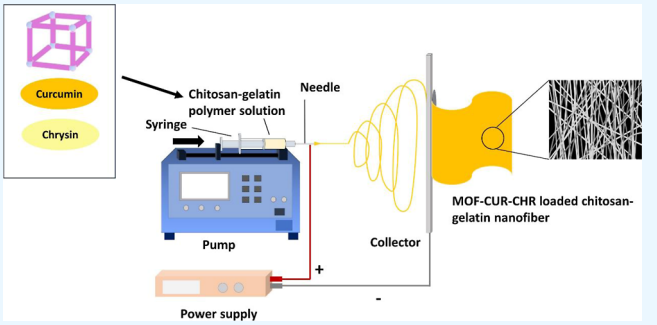

1. INTRODUCTION

Antibacterial wound dressings act as wound covers to reduce the risk of wound infections in partial- and full-thickness.[1] A nanofiber is defined as one-dimensional nanomaterials of a fiber shape with a diameter in the range of nanometers.[2] As an alternative to traditional wound dressing (gauze and bandages), the nanofiber has been devoted much attention due to its high porosity, biodegradability, and high surface-to-volume ratio.[3]

In addition to this, the nanofiber forms a structure similar to the natural extracellular matrix, promoting cell adhesion and proliferation and leading to an accelerated wound healing process.[4] In the past decade, the chitosan (CS)-gelatin (GL)-based nanofiber has attracted much attention in the field of drug delivery, wound care, as a biosensor, tissue engineering, and food packaging.[5] Blending of GL with CS improves the stability and the poor electrospinning ability of CS to produce nanofibers with better thermal and mechanical properties.[6]

Over the years, curcumin (CUR) or (bis-1,7-[4-hydroxy-3-methoxyphenyl]-hepta-1,6-dione) is a natural component of rhizome *Curcuma longa*.[7] This hydrophobic polyphenolic pigment has been widely used for medicinal purposes due to its antibacterial, antioxidant, anti-inflammatory, antifungal, antitumor, and wound healing effect.[8] Previous research has reported that CUR possesses a synergistic effect with flavonoids such as chrysin.[9−11] Chrysin (CHR) (5,7-dihydroxyflavone) belongs to a group of natural polyphenols, which occurs in honey and propolis, passion flowers, *Passiflora caerulea* and *Passiflora incarnata*, as well as in *Oroxylum indicum*.[12] Similar to CUR, CHR has shown various promising pharmacological effects, such as antimicrobial, anti-inflammatory, anticancer, and antidiabetic.[13]

The nanofiber is used as a nanocarrier to cope with the limitations of CUR and CHR, such as poor water solubility, low permeability, and bioavailability.[12,14] Despite the fact that

Received: September 3, 2024
Revised: April 22, 2025
Accepted: May 5, 2025
Published: May 22, 2025

https://doi.org/10.1021/acsomega.4c08100
ACS Omega 2025, 10, 21065−21076

the nanofibers have garnered considerable interest in drug delivery systems, the explosive release of nanofibers remains as a barrier to their use.[4] When the drug molecules are evenly distributed over the nanofiber surface, it results in a fast drug release.[4,15] In this present study, CUR and CHR were loaded into the presynthesized Hong Kong University of Science and Technology-1 (HKUST-1) or Cu-MOF to obtain modified CUR- and CHR-loaded Cu-MOFs (Cu-MOF-CUR-CHR). A metal−organic framework (MOF) is an extensive class of crystalline materials formed by inorganic metal ions and organic linkers by different methods such as the solvothermal method.[16] The MOF acts as an exceptional drug carrier with a superior loading capacity due to its highly ordered, porous, and 3-dimensional crystalline structure.[17] The Cu-MOF or HKUST-1, which is a copper-based MOF made up of dimeric Cu^{2+} units with 1,3,5-benzenetricarboxylic acid, has been widely used to act as a drug delivery vehicle in the biomedical field.[18] The combination of the MOF and nanofiber, which creates a unique class of hierarchical nanostructures, is able to cater the burst release of the polymer nanofiber by slowing the drug release.[15] Previously, Wang et al. reported that the polyacrylonitrile (PAN) composite nanofiber loaded with a *Portulaca oleracea* L. extract (POE) and a zinc-MOF slowed down the cumulative drug release from 90.54 ± 0.79% for the nanofiber without the MOF to 65.92 ± 1.95% for nanofibers with the MOF in 72 h.[19] However, the MOF nanofiber design remains limited in the existing field of drug delivery systems.

Herein, we aim to synthesize the electropsun CS-GL nanofiber loaded with Cu-MOF-CUR-CHR to test for its physiochemical properties using scanning electron microscopy (SEM), Fourier-transform infrared (FTIR) spectroscopy, and in vitro drug release behavior. In addition to the biocompatibility test, this study also evaluated the antibacterial efficacy of CS-GL/Cu-MOF-CUR-CHR nanofibers to compare them with CS-GL/CUR-CHR nanofibers. It is expected that these results provide as an impetus for further research on the synergistic effect of CUR and CHR with respect to the antibacterial effect for accelerating the wound healing process.

2. MATERIALS AND METHODS

2.1. Materials. Chitosan (low-molecular weight), gelatin from the bovine skin (Type B), curcumin powder from *C. longa* (turmeric), chrysin (97% 5, 7-dihydroxyflavone), thiazolyl blue tetrazolium bromide (MTT), dimethyl sulfoxide (99.9%, analytical reagent grade), copper(II) nitrate trihydrate, trimesic acid (BTC, benzene-1, 3, 5 tricarboxylic acid, H_3BTC), and glutaraldehyde solution (GTA, grade II, 25% H_2O) were purchased from Sigma-Aldrich (USA). Ethyl alcohol (95%, v/v- denatured) and acetic acid (Glacial, Analytical reagent) were purchased from SYSTERM-chemAR (Malaysia). For the preparation of phosphate-buffered solution (PBS), sodium chloride, potassium chloride, disodium hydrogen phosphate, and potassium dihydrogen phosphate were purchased from Merck (Germany). Dulbecco's Modified Eagle Medium (DMEM) and Human epidermal keratinocyte cell line (HaCaT) were procured from CLS-Cell Line Services (Germany). Trypsin (0.25%, 2.21 mM EDTA, 1× [−] sodium bicarbonate) was purchased from Thermo Fisher Scientific (U.S). The fetal bovine serum (FBS) was purchased from Eurobio Scientific (France). Penicillin−Streptomycin (100×) was purchased from MedChemExpress (USA). *Staphylococcus aureus* American Type Culture Collection (ATCC) 43300 and *Pseudomonas aeruginosa* ATCC 27853 were purchased from the ATCC (USA). Brain heart infusion (BHI) agar was purchased from Oxoid (United Kingdom).The soybean casein digest medium with tween 80 and lecithin (SCDLP) was purchased from HiMedia Laboratories (India). The nutrient broth (for microbiology) was purchased from Merck (Germany). All chemicals were used without additional purification.

2.2. Cu-MOF Synthesis. First, HKUST-1 or Cu-MOF was synthesized by using the solvothermal method as reported by Mohammadnejad and Fakhrefatemi.[20] To an amount of 7 mmol of copper(II) nitrate trihydrate in 15 mL of distilled water, 1.75 mmol of H_3BTC in 15 mL 95% ethanol was added.[21] After stirring at room temperature for 30 min, the reaction mixture was introduced into a Teflon-lined autoclave and heated at 140 °C for 24 h. After the heating process, the Cu-MOF product synthesized was rinsed with 15 mL of distilled water. The supernatant was discarded after centrifugation (5000XG, 30 min). The washing steps were repeated at least three times. Following this, the Cu-MOF product was rinsed with 15 mL of 95% ethanol at least three times to purify the Cu-MOF powder. After the supernatant was removed after centrifugation, the Cu-MOF powder was dried at 70 °C for 24 h.

2.3. Postsynthesis Modification of Cu-MOF with CUR and CHR. After the Cu-MOF synthesis, the presynthesized Cu-MOF was modified with CUR and CHR based on Lawson et al. with slight modification.[22] To prepare Cu-MOF-CUR-CHR, 5 g of each CUR and CHR (100 wt %) was dissolved in 500 mL of 95% ethanol to obtain a final concentration of 10 mg/mL followed by the addition of 10 g of Cu-MOF. The weight ratio of drugs to the Cu-MOF was kept at 1:1.[23] The mixture was stirred for 72 h at 350 rpm and 25 °C. After that, the impregnated Cu-MOF was recovered by centrifugation at 5000 XG for 30 min, and the supernatant was used to quantify the percentage encapsulation efficiency (EE). The modified Cu-MOF was rinsed with 15 mL of distilled water at least three times following that the supernatant was removed. After the drying process at 70 °C for 24 h, the dried Cu-MOF-CUR-CHR were added into a polymer solution for electrospinning to obtain nanofibers for further testing.

2.4. EE of CUR and CHR in Cu-MOFs. To quantify the amount of CUR and CHR within the Cu-MOF, the absorbance value of the supernatant collected was measured using a UV spectrophotometer at 425 nm (CUR)[24] and 275 nm (CHR).[25] The percentage of encapsulation efficiency (EE) was calculated using the below equation.

$$\text{Encapsulation efficiency (\%)} = \left(\frac{\text{Entrapped drug}}{\text{Total drug added}}\right) \times 100$$

2.5. Preparation of CS-GL/CUR-CHR and CS-GL/Cu-MOF-CUR-CHR Polymer Solution. Based on Ahmadi et al. with slight modification,[6] CS 2 wt % and GL 45 wt % in 25% acetic acid with a ratio of 30/70 (CS: GL)[26] were prepared and stirred at 50° C for 1 h. To prepare the CS-GL/CUR-CHR polymer solution, 1, 5, 10, and 20 wt % of pure CUR and CHR (ratio 1:1, with respect to the CS-GL content) were added into the CS-GL polymer solution.[11] Similarly, CS-GL/Cu-MOF-CUR-CHR polymer solutions with 1, 5, 10, and 20 wt % were prepared in the ratio of the synthesized Cu-MOF-CUR-CHR to CS-GL content (1:1). After being stirred for 1 h at 50 °C, the prepared polymer solutions were then sonicated for 5 min before electrospinning was performed.

https://doi.org/10.1021/acsomega.4c08100
ACS Omega 2025, 10, 21065−21076

2.6. Electrospinning and Cross-Linking Using Glutaraldehyde (GTA) Vapor Treatment. To form a nanofiber, the prepared blend solution was transferred into a 5 mL syringe and connected to a needle gaged 22 G. After that, the electrospinning process was performed at a flow rate of 0.8 mL/h, 15 cm nozzle-to-collector, and 18 kV voltage for 2 h. The nanofiber formed on the collector was dried at 70 °C for 24 h to remove the additional solvent. Following this, the cross-linking of the CS-GL nanofiber was performed by using GTA vapor treatment at 25 °C according to Hajzamani et al.[27] First, 10 mL of GTA and nanofibers was taken in a closed container for 24 h. After cross-linking, the nanofiber was dried overnight at 70 °C to remove entrapped GTA.

2.7. ATR-FTIR Spectroscopy. To determine the chemical structures of copper, trimesic acid, Cu-MOF, CS-GL nanofiber, CS-GL/CUR-CHR, and CS-GL/Cu-MOF-CUR-CHR nanofibers, the FTIR spectra of each sample were obtained using a Shimadzu IRAffinity-1S machine equipped with an attenuated total reflection (ATR) accessory with a diamond crystal at an angle of incidence 45°. The samples were directly placed onto the diamond crystal and subjected to FTIR spectroscopy scanning. The FTIR study was carried out at a scan rate of 16 scans and wavenumbers ranging from 4000 to 400 cm^{-1}, with 4 cm^{-1} resolutions.

2.8. Scanning Electron Microscopy (SEM). To investigate the morphology and diameter of nanofibers, a JEOL 6400 scanning electron microscope (SEM) was attached with Energy-Dispersive X-ray (EDX) (Microscopy Unit. Institute of Bioscience, University Putra Malaysia, Malaysia) at 5 kV was used. After coating the samples with gold using a Bal-Tec SCD005 Sputter-Coater, the samples were observed and analyzed by SEM. Following this, the diameter of the nanofiber (n = 50) was measured using ImageJ software (Version 1.53 K).

2.9. EE of CUR and CHR within Electrospun CS-GL Nanofibers. First, a 2.5 cm × 2.5 cm nanofibrous scaffold was prepared and immersed in 10 mL of 95% ethanol for 6 h at room temperature. After the dissolution of CUR and CHR, the absorbance of solutions was measured using a Shimadzu UV-1800 UV−visible scanning spectrophotometer at 425 nm[24] and 275 nm[25] for CUR and CHR, respectively. The absorbance obtained was applied to the calibration curve to calculate the total drug load content or the amount of drug released in ethanol. All the tests were performed in triplicate and their average was taken. The encapsulation efficiency of CUR and CHR in nanofibers was calculated using the following formula

$$\text{encapsulation efficiency}(\%) = \left(\frac{\text{total drug load content in nanofibers}}{\text{total amount of the inital drug}}\right) \times 100$$

2.10. In Vitro Drug Release. To conduct a drug release test, a 2.5 cm × 2.5 cm nanofiber was cut and immersed in 10 mL of PBS solution (pH 7.4) at 37 °C with a rotating speed of 100 rpm. At each time point (10, 20, 30, 1, 2, 4, 6, 12, 24, and 48 h), 5 mL of samples were withdrawn by a 10 mL Terumo syringe. At each sampling process, 5 mL of a fresh PBS solution was returned to maintain a constant volume of media. The calibration curves at 423 nm[28] and 267 nm[29] were used to measure the amount of CUR and CHR released from nanofibers in the PBS solution (pH 7.4). All tests were performed in triplicate and the average was obtained. The percentage of released CUR and CHR at each time interval was calculated based on the equation below

$$\text{drug release}(\%) = \left(\frac{\text{total amount of drug released in PBS}}{\text{total drug load content in ethanol}}\right) \times 100$$

2.11. Cell Viability Test. The cell viability test of nanofibers was performed by using an MTT assay.[30] First, a 2.5 cm × 2.5 cm nanofiber was cut and irradiated under UV light for 30 min. The test samples and controls, such as polyethylene (PE) and zinc diethyldithiocarbamate (ZDTC), were placed into the wells.[31] The irradiated nanofibers and controls were added with 1 mL of Dulbecco's modified Eagle's medium (DMEM) supplemented with 10% (v/v) FBS, 1% penicillin/streptavidin in a 12-well culture plate, and incubated at 37 °C for 48 h. The PE acted as the negative control while the ZDTC served as the positive control to verify that the experimental procedure was functioning as expected.[31] Then, HaCaT cells were seeded at a density of 5000 cells/mL in 96-well culture plates for 24 h. After that, the medium was removed and replaced with a soaked solution of nanofibers. The plate was then incubated at 37 °C for 48 h. Following this, a 25 μL of 2 mg/mL MTT reagent was added into each well and incubated at 37 °C for 3 h. After 3 h of incubation, the solution was discarded. One hundred microliters of DMSO were added into each well to dissolve the formed formazan crystal. The absorbance of the solution was measured at 570 nm by using a microplate reader. The control used in this experiment was the cells added to the fresh medium without a sample. The experiment was performed in triplicate.

$$\text{Cell viability}(\%) = \left(\frac{\text{OD control} - \text{OD sample}}{\text{OD control}}\right) \times 100$$

2.12. Antibacterial Test. The antibacterial effect of nanofiber against *S. aureus* ATCC 29213 and *P. aeruginosa* ATCC 27853 was carried out by using the colony counting method.[32] Initially, a 2.5 cm × 2.5 cm nanofibrous scaffold was irradiated under UV light for 30 min. Each bacterium was plated on a brain heart infusion (BHI) agar plate overnight at 37° C. Colonies of each bacterium were picked and dissolved in a nutrient broth (ratio of 1/500). The bacterial suspension was measured at $OD_{625\ nm}$ using a microplate reader to obtain an OD of 0.12 (10^8 cfu/mL). 10-fold dilutions were performed by transferring 100 mL of adjusted bacterial suspension into 900 μL of the nutrient broth. Following this, 20 microliters of the suspension (1×10^5 cfu/mL) were added to the irradiated nanofiber and covered with a sterile coverslip. After 3 h incubation at room temperature, the nanofiber was transferred into a 5 mL centrifuge tube and added with 1 mL of soybean-casein-digest-lecithin-polysorbate 80 (SCDLP); thereby, the tube was vortexed for 60 s. Two hundred microliters of the solution were extracted into 96 well culture plates. Five serial dilutions were performed, and 10 μL of each dilution was spotted on the BHI agar plate. After 24 h incubation at 37 °C, the colonies were counted manually to calculate the number of colony-forming units per milliliter (cfu/mL). The CS-GL nanofiber was used as a control in the calculation of $\log_{10}$ reduction values (LRVs). The LRV was calculated using the equation below

https://doi.org/10.1021/acsomega.4c08100
ACS Omega 2025, 10, 21065−21076

logarithm reduction values (LRV)

$$= \log_{10}\text{cfu/mLsample} - \log_{10}\text{cfu/mLcontrol}$$

(CS − GLnanofibers)

2.13. Statistical Analysis. For comparison of relative groups, statistical analysis was conducted with the Student's *t*-test by using Statistical Package of Social Sciences (SPSS, IBM, version 28) software. All the samples were considered significant with * *p*-value ≤0.05 and ** (*p*-value ≤0.01).

3. RESULTS AND DISCUSSION

3.1. Synthesis and Characterization of Cu-MOF-CUR-CHR. In this study, CUR and CHR were loaded to the presynthesized Cu-MOF using the postsynthesis modification method. As shown in Table 1, we obtained Cu-MOF-CUR-CHR with a high encapsulation efficiency of 99.2% for both CUR and CHR, which was higher than the % EE of CUR in the Zn-MOF (79.2%) obtained by Nabipour et al.[33] This also indicated the higher drug loading[34,53] capacity of Cu-MOF than Zn-MOF. Additionally, ATR-FTIR analysis was used to confirm the presence of CUR and CHR within the CS-GL nanofiber.

Table 1. Encapsulation Efficiency (% EE) of CUR and CHR within Cu-MOFs

samples	EE of CUR (%)	EE of CHR (%)
Cu-MOF-CUR-CHR	99.2 ± 0.011	99.2 ± 0.036

The formation of the Cu-MOF involves the bonding of copper(II) nitrate trihydrate and trimesic acid (H_3BTC). In the Cu-MOF spectrum shown in Figure 1A, the absorption peaks located at 1643 cm^{-1}, 1369 cm^{-1}, and 729 cm^{-1} corresponded to the O−H stretching vibration in the adsorbed H_2O molecule in $Cu_3(BTC)2$, the O═C−O bonded to Cu, the C═C stretching vibration of the aromatic rings of BTC molecules, and the Cu−O stretching vibration, respectively. These stretching vibrations closely match data previously published in the literature.[35] Based on Figure 1B, several common peaks have been seen for CS and GL such as a broad peak at 3358 and a weak peak at 2900 cm^{-1} representing the groups of O−H and CH_2, respectively. To demonstrate the presence of CS and GL in the CS-GL nanofiber, distinct peaks of CS at 1080.14 cm^{-1} and GL at 1631 cm^{-1} and 1529 cm^{-1} appeared in the spectra. These results were in accordance with previous findings.[6,36]

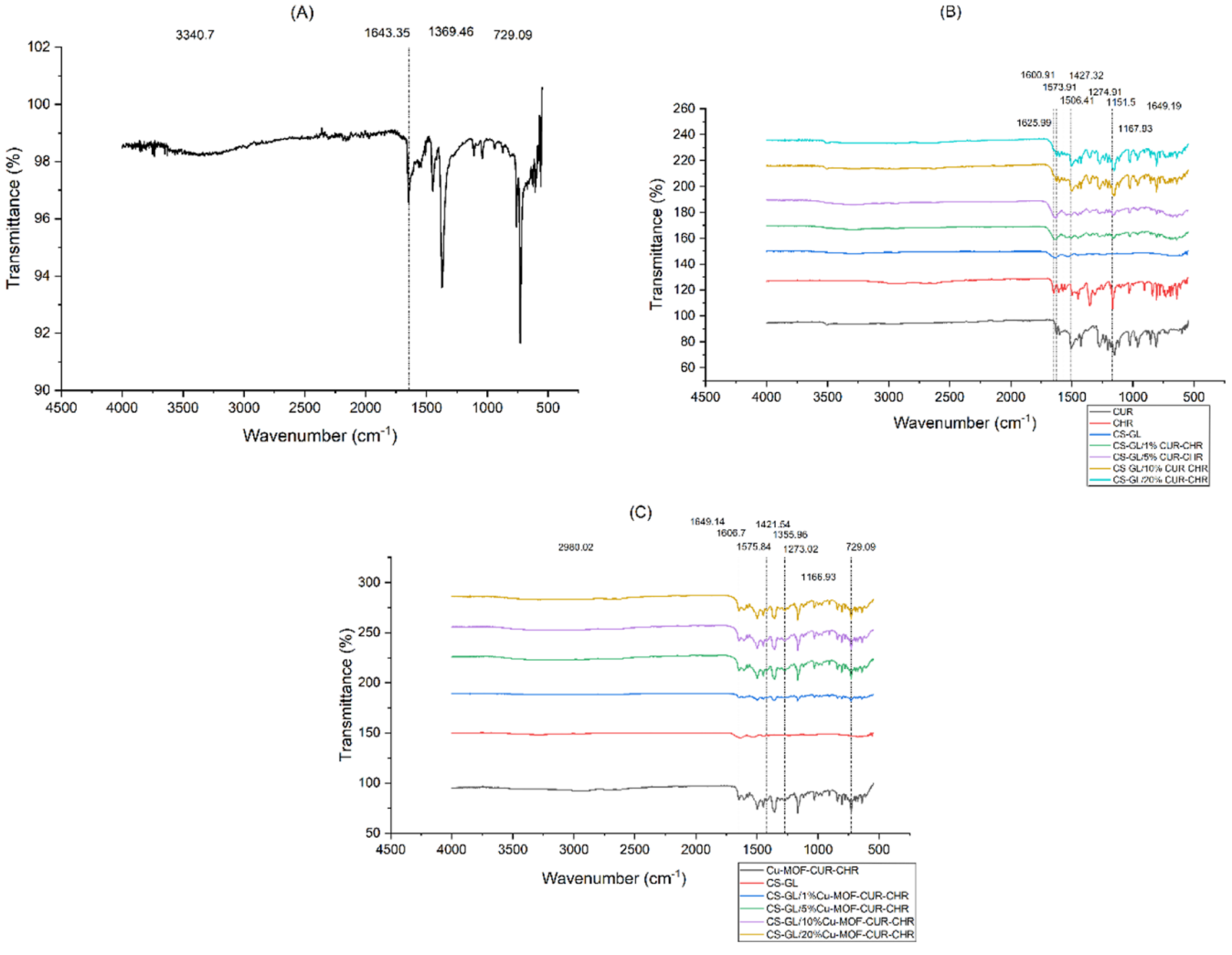

Figure 1. FTIR spectra of (A) Cu-MOF, (B) CS-GL/CUR-CHR nanofiber, and (C) CS-GL/Cu-MOF-CUR-CHR nanofibers.

https://doi.org/10.1021/acsomega.4c08100
ACS Omega 2025, 10, 21065−21076

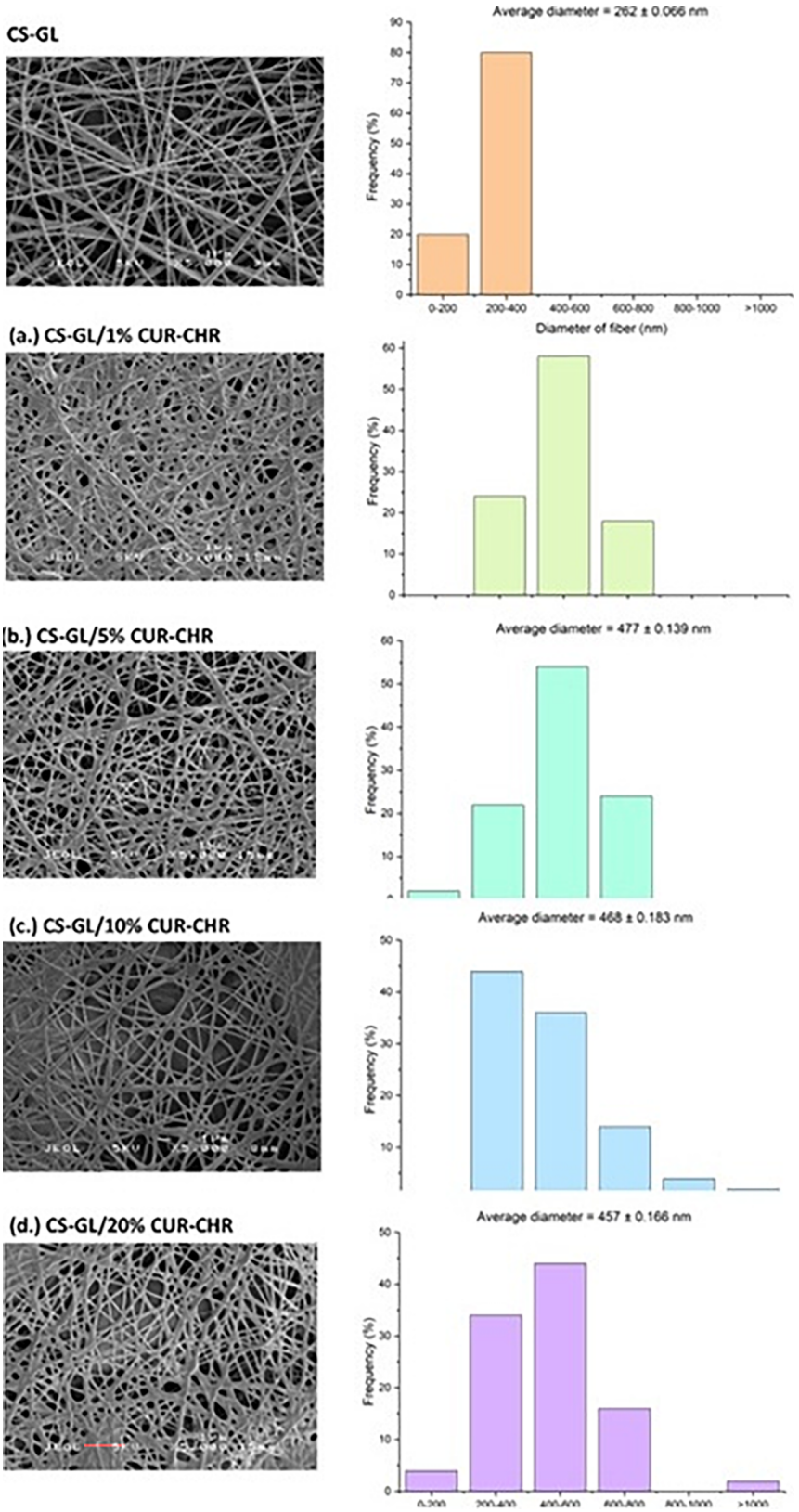

Figure 2. continued

https://doi.org/10.1021/acsomega.4c08100
ACS Omega 2025, 10, 21065−21076

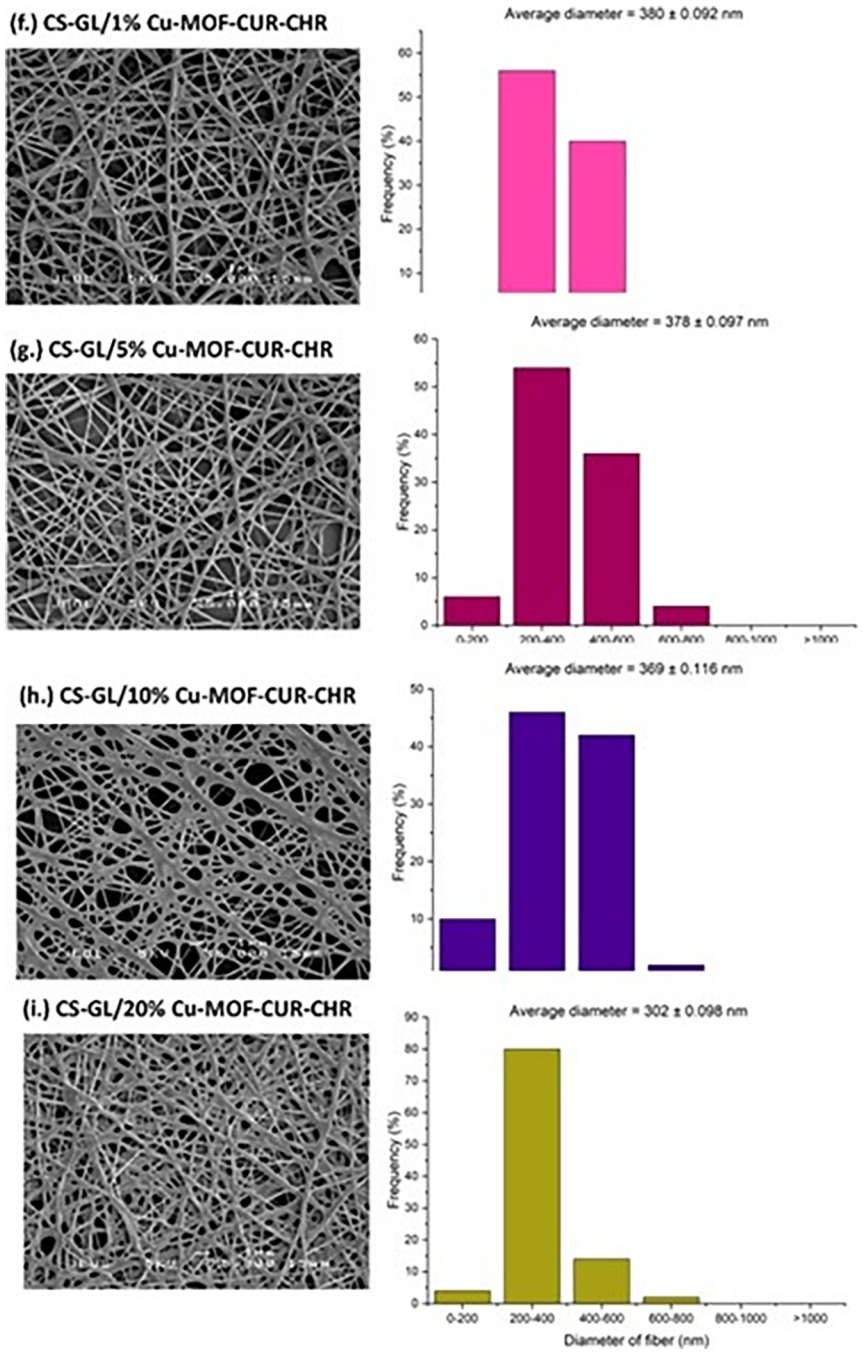

Figure 2. SEM images, nanofiber diameter distribution, and the average diameter of CS-GL/CUR-CHR and CS-GL/Cu-MOF-CUR-CHR nanofibers with four different drug concentrations.

The FTIR spectra of the samples obtained after drug encapsulation into the CS-GL polymer blend were comparatively studied. The peak shifting of functional groups provides an excellent way to determine the extent of encapsulation when the FTIR spectra of the polymer-encapsulated drug, the free drug, and the polymer-free drug were compared. In the spectra of all CS-GL/CUR-CHR nanofibers, the prominent peaks at 1448 cm^{-1} and 1273 cm^{-1} appeared to belong to CUR, while the peaks at 1571 cm^{-1}, and 1184 cm^{-1} observed belong to CHR. Compared to native drugs and polymers, there was no major shift of functional peaks, showing that there were no significant interactions between drugs and polymers that could alter the effective nature of the functional group. By increasing the drug concentrations up to 10% and 20%, more absorption peaks for CUR (1625 cm^{-1} and 1602 cm^{-1}) and CHR (2628 cm^{-1}) were identified.[9,37] In addition, CHR was observed in the spectra of CS-GL/CUR-CHR nanofibers due to the incorporation of CUR and CHR into the CS-GL nanofiber. This suggested the true interactions between CUR and CHR with the CS-GL nanofiber.

Based on the comparison of FTIR spectra of the free drug and Cu-MOF, it demonstrated the characteristics peaks for the Cu-MOF (1355 cm^{-1} and 729 cm^{-1}), CUR (1606 cm^{-1}, 1421 cm^{-1}, and 1273 cm^{-1}), and CHR (2980 cm^{-1}, 1575 cm^{-1}, and 1166 cm^{-1}).[38] It was found that the common needle-like peak of the Cu-MOF and CHR overlapped at 1649 cm^{-1}. Hence,

https://doi.org/10.1021/acsomega.4c08100
ACS Omega 2025, 10, 21065−21076

these data represented the successful encapsulation of CUR and CHR into the MOF.

In Figure 1C, all the CS-GL/Cu-MOF-CUR-CHR nanofibers contained the absorption bands for the existence of the MOF (1647 cm^{-1}, 1355 cm^{-1}, and 729 cm^{-1}), CUR (1448 cm^{-1} and 1273 cm^{-1}), and CHR (1577 and 1168 cm^{-1}). In the CS-GL/Cu-MOF-CUR-CHR nanofiber, the absorption peak of CUR shifted from 1421 cm^{-1} to 1448 cm^{-1}. The FTIR spectra revealed that the prominent peaks for the Cu-MOF and CUR overlapped at 1647 cm^{-1}. Compared to other concentrations of CS-GL/Cu-MOF-CUR-CHR nanofibers, there was a loss of one absorption band at 2989 cm-1 in 1% CS-GL/Cu-MOF-CUR-CHR nanofibers. Due to a high drug concentration within nanofibers, additional peaks were identified clearly at the spectra of the nanofibers with higher drug concentrations.

3.2. Scanning Electron Microscopy (SEM). After the characterization of Cu-MOF-CUR-CHR, we loaded the Cu-MOF-CUR-CHR into the CS-GL polymer solution to fabricate the nanofiber using the electrospinning technique. Nanofibers with different drug contents were characterized using scanning electron microscopy (SEM). The SEM images demonstrated that all the nanofibers met the requirement in engineering a hybrid scaffold by showing the nanofibers were porous, uniform in size, and had fewer beads.[39] The high porosity of nanofibers prevents bacterial infection and provides moisture to allow the transfer of nutrient and oxygen exchange.[40]

Compared to the control (CS-GL nanofibers), the average diameter of the CS-GL nanofiber was increased with the addition of CUR and CHR. The increased average diameter indicated the effect of the filling nature of CUR and CHR as additional components in the spinning solution. This effect on the average diameter nanofiber was consistent with previous studies.[41,42] As shown in Figure 2, the average diameter directly depended on the initial CUR and CHR loaded into the nanofiber. Similar to previous findings,[42,43] the average diameter decreased with the increase of CUR and CHR contents. Additionally, the average diameter of CS-GL/Cu-MOF-CUR-CHR nanofibers was lower than that of CS-GL/CUR-CHR nanofibers. This could be due to the presence of the Cu-MOF decreasing the average diameter of nanofibers by decreasing the viscosity of the polymer solution. Therefore, this allows the formation of more uniform and smaller nanofibers than those without the Cu-MOF.[44]

3.3. The Encapsulation Efficiency of CUR and CHR of Nanofibers. As shown in Table 2, the percentage of drug encapsulation efficiency for CS-GL/Cu-MOF-CUR-CHR nanofibers was higher than that for CS-GL/CUR-CHR nanofibers. Accordingly, the drug encapsulation efficiency of Cu-MOFs was better than the CS-GL blend due to the large pore volume, highly ordered structure, and high surface area-to-volume ratio offered by Cu-MOFs.[22] This allows the Cu-MOF to adsorb large amounts of drug molecules and trap them inside the framework.[45] Additionally, the percentage of the encapsulation efficiency of all nanofibers increased with an increase in drug contents. The CUR was encapsulated in the CS-GL nanofiber with an EE value higher than that of the CHR in both CS-GL/CUR-CHR and CS-GL/Cu-MOF-CUR-CHR nanofibers. This could be due to the lower solubility of CHR than CUR causing the lesser amount of CHR dissolving in the CS-GL polymer blend.[46] Furthermore, it was found that the CS-GL/Cu-MOF-CUR-CHR nanofiber with more than 1% drug content resulted in 100% EE for both CUR and CHR. From our data, the CS-GL/Cu-MOF-CUR-CHR nanofiber showed a higher EE for CUR and CHR than that for previous findings that used a single drug in nanofibers without Cu-MOFs.[47]

Table 2. Encapsulation Efficiency (% EE) of CUR and CHR within Electrospun Drug-Loaded CS-GL Nanofibers

samples	EE for CUR (%)	EE for CHR (%)
CS-GL/1% CUR-CHR	11.96 ± 0.181	10.91 ± 0.199
CS-GL/5% CUR-CHR	17.29 ± 0.320	13.00 ± 0.319
CS-GL/10% CUR-CHR	19.22 ± 6.400	15.18 ± 0.286
CS-GL/20% CUR-CHR	38.35 ± 0.764	27.15 ± 2.519
CS-GL/1% Cu-MOF-CUR-CHR	97.12 ± 3.672	91.68 ± 1.310
CS-GL/5% Cu-MOF-CUR-CHR	108.81 ± 5.745	103.56 ± 7.415
CS-GL/10% Cu-MOF-CUR-CHR	107.95 ± 0.615	100.92 ± 2.016
CS-GL/20% Cu-MOF-CUR-CHR	103.40 ± 4.166	100.67 ± 2.934

3.4. In Vitro Drug Release of Nanofibers. In Figure 3, all CS-GL/CUR-CHR nanofibers showed initial CUR and CHR releases after 20 min, while the initial drug release of CS-GL/Cu-MOF-CUR-CHR nanofibers was detected after 10 min. The initial CUR release of CS-GL/1% Cu-MOF-CUR-CHR nanofibers (23.7%) was the highest among the samples (5, 10, and 20%). This data was higher than the % cumulative release (12.9%) obtained by Fahimirad et al. in the first 2 h.[48] However, the initial CHR release of CS-GL/Cu-MOF-CUR-CHR increased from a range of 13.7 ± 9.222% to 15.5 ± 0.578% as the drug concentration increased in the nanofiber. Importantly, the maximum drug release of CS-GL/Cu-MOF-CUR-CHR nanofibers was higher compared to that of CS-GL/CUR-CHR nanofibers. Based on the data, the maximum drug release from the nanofiber is correlated to the amount of drug loaded into the nanofiber. Furthermore, CUR release was higher than that of CHR in all nanofibers. Faster drug release kinetics was observed in CS-GL/CUR-CHR nanofibers by showing their maximum release within 6 h. In contrast, the presence of Cu-MOFs within the nanofiber resulted in high and prolonged drug release up to 48 h. The prolonged drug release of the nanofiber with the Cu-MOF may be attributed to the CS-GL nanofiber protecting the drug molecules leaked out from the Cu-MOF to keep the drug molecules within the delivery system.[49]

3.5. Cell Viability Test. Figure 4 shows the effect of CS-GL/CUR-CHR and CS-GL/Cu-MOF-CUR-CHR nanofibers with different concentrations on the % cell viability of HaCaT cells after 48 h. Similar results of the PE and ZDTC were seen in previous research conducted by Sreekantan et al.[31] Based on Figure 5, all nanofibers exhibited a higher cell viability than ZDTC (5.8 ± 0.092%). Importantly, the addition of Cu-MOF alone (1−20%) into CS-GL nanofibers showed no cytotoxicity, implying the low toxicity of Cu-MOFs in human cells (Figure S1). In addition, our data revealed that not all nanofibers exhibited significant toxicity as CS-GL/CUR-CHR and CS-GL/Cu-MOF-CUR-CHR nanofibers with 1% and 5% of drug concentrations achieved more than 70% cell viability. The MTT value showed that all nanofibers with 10% and 20% drug concentrations were more cytotoxic than those with 1% and 5% drug concentrations. By increasing the % drug concentration by more than 5%, the cell viability of the nanofiber decreased. Hence, the data reported that CS-GL/CUR-CHR and CS-GL/Cu-MOF-CUR-CHR nanofibers with 1% and 5%

https://doi.org/10.1021/acsomega.4c08100
ACS Omega 2025, 10, 21065−21076

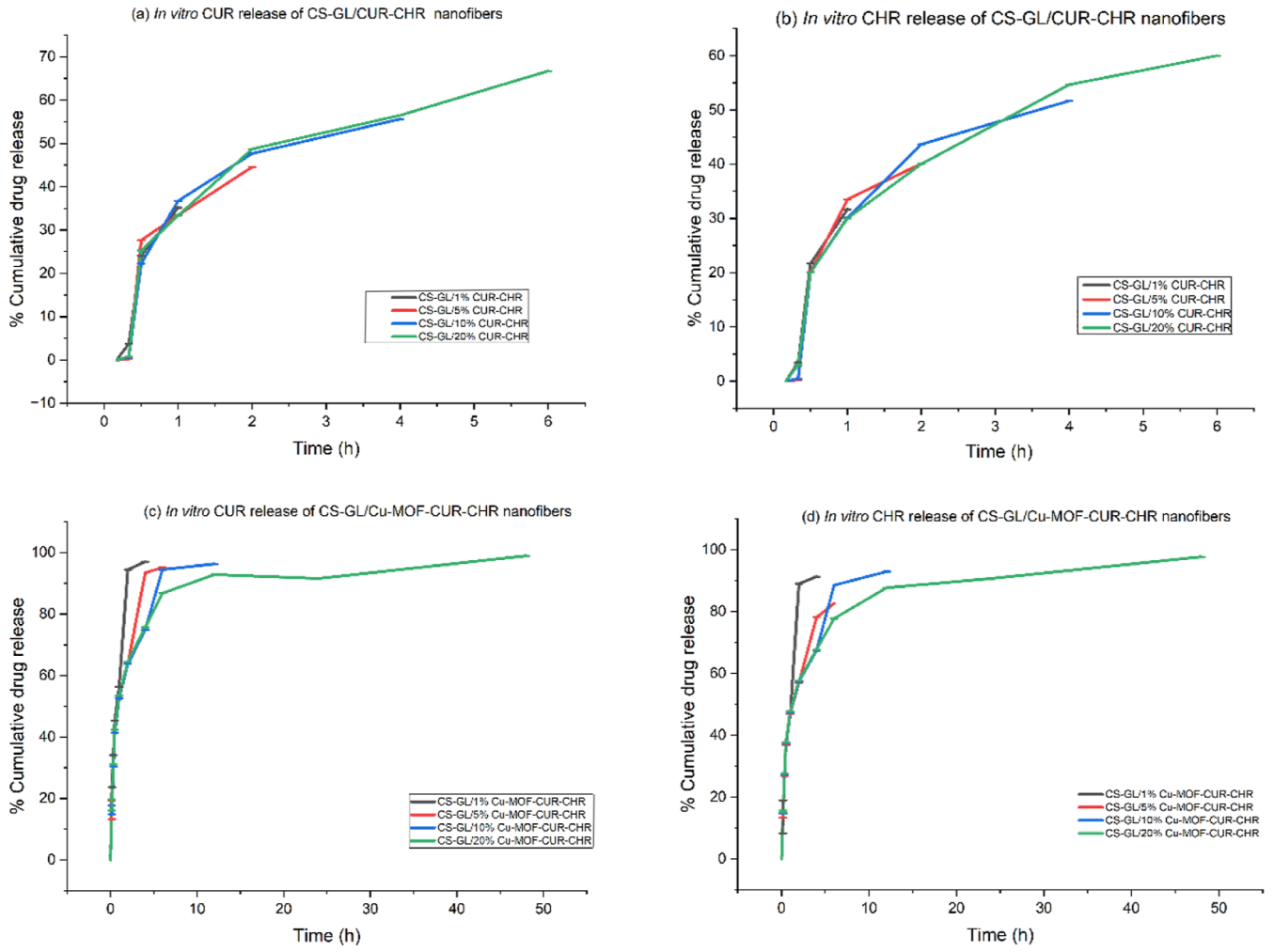

Figure 3. Drug release behavior of CUR and CHR from CS-GL/CUR-CHR (a,b) and CS-GL/Cu-MOF-CUR-CHR (c,d) nanofibers in PBS at pH 7.4.

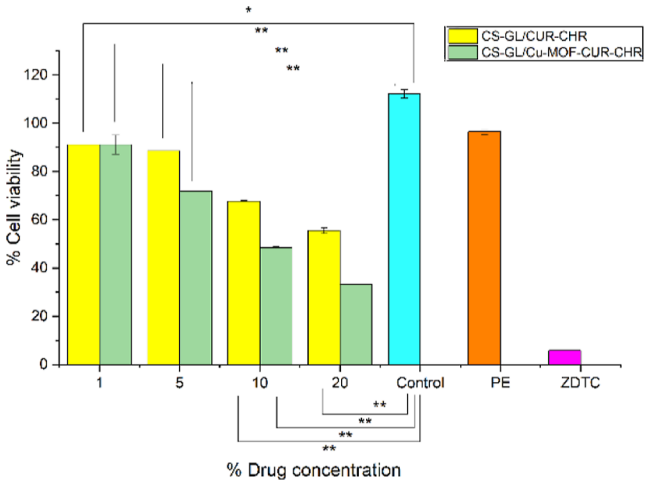

Figure 4. % Cell viability of CS-GL/CUR-CHR and CS-GL/Cu-MOF-CUR-CHR nanofibers. Control: without sample; PE: polyethylene; and ZDTC: zinc diethyldithiocarbamate. * Significant differences between the CS-GL (control) and CS-GL/CUR-CHR and CS-GL/Cu-MOF-CUR-CHR groups (p-value ≤0.05) and ** (p-value ≤0.01).

of drug concentrations were considered biocompatible materials due to their high cell viability (>70%). Nonetheless, the data showed that CS-GL/Cu-MOF-CUR-CHR nanofibers ($p \leq 0.01$) exhibited lower cell viability than CS-GL/CUR-CHR nanofibers ($p \leq 0.001$). For example, CS-GL/Cu-MOF-CUR-CHR nanofibers with 10% and 20% drug concentrations exhibited the lowest % cell viability (48.3% ± 0.913 and 33.3% ± 0.123, respectively) among the nanofibers. This may be due to the higher drug loading within CS-GL/Cu-MOF-CUR-CHR than CS-GL/CUR-CHR causing the reduced cell viability.

3.6. Antibacterial Test. The CS-GL/CUR-CHR and CS-GL/Cu-MOF-CUR-CHR nanofibers with more than 70% cell viability were selected to perform the antibacterial test against *S. aureus* and *P. aeruginosa*. In this study, *S. aureus* and *P. aeruginosa*, which are the most common causes of wound infection, were selected for the antibacterial test. *S. aureus* is a Gram-positive bacterium that causes most infections such as skin infections.[50] *P. aeruginosa* is a Gram-negative bacterium that infects patients with cystic fibrosis, burn wounds, and severe infection.[51] The antibacterial effect of the selected nanofibers was evaluated by determining the number of colonies ($\log_{10}$ cfu/mL) and LRV. Based on Table 3, the data showed that the effectiveness of all nanofibers selected in inhibiting *S. aureus* (LRV of 2.69 ± 0.030) was greater than that of *P. aeruginosa* (1.87 ± 0.564). Additionally, the antibacterial effect of nanofibers was enhanced with the

https://doi.org/10.1021/acsomega.4c08100
ACS Omega 2025, 10, 21065−21076

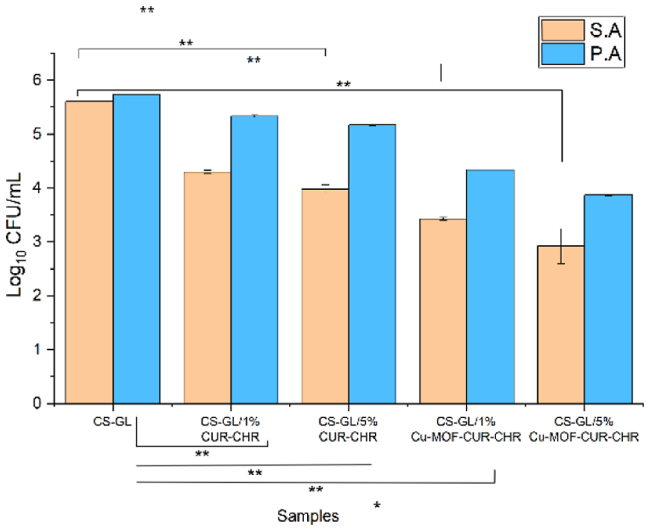

Figure 5. Antibacterial effect (logarithm of number of colony-forming units per milliliter, cfu/mL) of selected nanofibers against *S.aureus* (S.A) and *P. aeruginosa* (P.A). Bacterial growth in CS-GL represents the control with bacteria strains devoid of drugs. * Significant differences between the CS-GL (control) and CS-GL/CUR-CHR and CS-GL/Cu-MOF-CUR-CHR groups (p-value ≤0.05), and ** (p-value ≤0.01).

Table 3. Logarithm Reduction Value (LRV) of Nanofibers[a]

	LRV	
samples	Staphylococcus aureus	Pseudomonas aeruginosa
CS-GL/1% CUR-CHR	1.31 ± 0.044	0.41 ± 0.056
CS-GL/5% CUR-CHR	1.62 ± 0.026	0.57 ± 0.130
CS-GL/1% Cu-MOF-CUR-CHR	2.18 ± 0.032	1.40 ± 0.051
CS-GL/5% Cu-MOF-CUR-CHR	2.69 ± 0.030	1.87 ± 0.564

[a]LRV = $\log_{10}$ cfu/mL sample − $\log_{10}$ cfu/mL control (CS-GL nanofibers).

increase in the concentration of CUR and CHR. Based on Figure 5, CS-GL/5% Cu-MOF-CUR-CHR had a higher antibacterial effect against *S. aureus* when the number of bacteria was decreased to 2.92 $\log_{10}$ cfu/mL (p-value ≤0.0001) compared to CS-GL/1% Cu-MOF-CUR-CHR (3.40 $\log_{10}$ cfu/mL, p-value ≤0.0001). Compared to CS-GL/CUR-CHR nanofibers, the antibacterial effect was significantly higher (p ≤ 0.05) in CS-GL/Cu-MOF-CUR-CHR nanofibers. From the data, the highest LRV value was observed (LRV of 2.69 ± 0.030 for *S. aureus* and 1.87 ± 0.564 for *P. aeruginosa*) in the CS-GL/5% Cu-MOF-CUR-CHR, indicating its strongest antibacterial effect among the samples. These results could be attributed to the Cu-MOF as a drug carrier with a high loading capacity facilitating the drug release to the bacteria to induce an efficient antibacterial effect.[52]

4. CONCLUSIONS

Due to the burst release of drugs from nanofibers, nanofibers still remain at the laboratory level. The formation of MOF nanofibers has advantages over conventional materials by reducing the rate of drug release. In this study, a biocompatible CS-GL nanofibers loaded with Cu-MOF-CUR-CHR was successfully fabricated. Incorporation of Cu-MOF-CUR-CHR with 99.2% of EE of CUR and CHR into CS-GL nanofibers reduced the fiber diameter in the range of 302 ± 0.098 to 380 ± 0.092 nm due to increased conductivity in the electrospinning process. In the FTIR spectra of Cu-MOF-CUR-CHR, it was proved that the CUR and CHR loading into HKUST-1 did not chemically change the bond structures of the Cu-MOF. Similarly, FTIR spectra of CS-GL/Cu-MOF-CUR-CHR nanofibers were unaffected by the impregnation of Cu-MOF-CUR-CHR into the CS-GL nanofiber by showing the retained characteristic peaks for Cu-MOF-CUR-CHR and CS-GL. For the drug release behavior of nanofibers in PBS at pH 7.4, the CUR and CHR releases of CS-GL/Cu-MOF-CUR-CHR nanofibers were sustained for up to 48 h, allowing prolonged antibacterial activity. The maximum cumulative release of CUR and CHR of about 97% was obtained from the CS-GL/20% Cu-MOF-CUR-CHR nanofiber after 24 h. Based on the results, CS-GL/5% Cu-MOF-CUR-CHR nanofibers exhibited the highest LRV (2.69 ± 0.030) against *S. aureus* (p-value ≤0.05). Therefore, it has the potential to be used as a therapeutic antibacterial wound dressing due to the role of Cu-MOF as a carrier for the sustained release of CUR and CHR over an extended period. In the future, CS-GL/Cu-MOF-CUR-CHR nanofibers are expected to be studied in human studies to act as an alternative to conventional wound dressing. Additionally, a pH-responsive antibacterial CS-GL/Cu-MOF-CUR-CHR nanofiber will be one of the major future directions for the treatment of acute and chronic wounds, depending on the pH of the skin.

■ ASSOCIATED CONTENT

Supporting Information

The Supporting Information is available free of charge at https://pubs.acs.org/doi/10.1021/acsomega.4c08100.

% cell viability of CS-GL/Cu-MOF nanofibers (PDF)

■ AUTHOR INFORMATION

Corresponding Authors

Soo Ghee Yeoh − *School of Postgraduate Studies, IMU University, 57000 Kuala Lumpur, Malaysia;* orcid.org/0009-0009-7143-8388; Email: 00000039958@imu.edu.my

Yoon Yee Then − *Department of Pharmaceutical Chemistry, School of Pharmacy, IMU University, 57000 Kuala Lumpur, Malaysia*; Email: thenyoonyee@imu.edu.my

Authors

Yun Khoon Liew − *Department of Life Sciences, School of Pharmacy, IMU University, 57000 Kuala Lumpur, Malaysia*

Wei Meng Lim − *School of Pharmacy, Monash University Malaysia, 47500 Subang Jaya, Selangor, Malaysia;* orcid.org/0000-0002-5076-9390

Norizah Abdul Rahman − *Department of Chemistry, Faculty of Science and Nanomaterials Processing and Technology Laboratory, Institute of Nanoscience and Nanotechnology, Universiti Putra Malaysia, 43400 Serdang, Selangor, Malaysia*

Complete contact information is available at: https://pubs.acs.org/10.1021/acsomega.4c08100

Author Contributions

Conceptualization, Y.Y.T.; Methodology, S.G.Y., Y.K.L., W.M.L., and Y.Y.T.; Validation, Y.K.L., W.M.L., and Y.Y.T.; Formal analysis, S.G.Y., Y.K.L., W.M.L., N.A.R., and Y.Y.T.; Investigation, S.G.Y., Y.K.L., W.M.L., and Y.Y.T.; Resources,

https://doi.org/10.1021/acsomega.4c08100
ACS Omega 2025, 10, 21065−21076

Y.Y.T.; Data curation, S.G.Y.; Writing and original draft, S.G.Y.; Writing and review and editing, Y.K.L., W.M.L., N.A.R., and Y.Y.T.; Visualization, S.G.Y. and Y.Y.T.; Supervision, Y.K.L., W.M.L., N.A.R., and Y.Y.T.; Project administration, Y.Y.T.; Funding acquisition, Y.Y.T. All authors have read and agreed to the published version of the manuscript.

Funding

This research was supported by the Fundamental Research Grant Scheme (FRGS) from the Ministry of Higher Education of Malaysia (Project reference code: FRGS/1/2022/STG05/IMU/02/1).

Notes

The authors declare no competing financial interest.

Biography

Soo Ghee Yeoh is a postgraduate student pursuing a MSc in Medical and Health Sciences at IMU University in Malaysia under the supervision of Yoon Yee Then and cosupervision of Yun Khoon Liew, Wei Meng Lim, and Norizah Abdul Rahman. Yun Khoon Liew is a Senior Lecturer at IMU University who focuses on Microbiology and Molecular biology. Wei Meng Lim is a Malaysian registered pharmacist, currently a lecturer at the School of Pharmacy, Monash University Malaysia. Norizah Abdul Rahman is an Associate Professor ChM at the Department of Chemistry, Faculty of Science, Universiti Putra Malaysia. Yoon Yee Then is a Senior Lecturer at IMU University, specializing in biomaterials science.

■ ACKNOWLEDGMENTS

The authors would like to acknowledge support from the Fundamental Research Grant Scheme (FRGS) from the Ministry of Higher Education of Malaysia (Project reference code: FRGS/1/2022/STG05/IMU/02/1). The authors are grateful to IMU University in providing the facilities and support for this project.

■ ABBREVIATIONS

cfu	colony forming unit
CHR	chrysin
CS	chitosan
CUR	curcumin
DMEM	Dulbecco's modified eagle medium
EE	encapsulation efficiency
FBS	fetal bovine serum
FTIR	Fourier transform infrared
GL	gelatin
GTA	glutaraldehyde
HKUST-1	Hong Kong University of Science and Technology-1
LRV	logarithm reduction value
MOF	metal−organic framework
MTT	3-(4,5-dimethylthiazol-2-yl)-2,5-diphenyltetrazolium bromide
PAN	polyacrylonitrile
POE	*Portulaca oleracea* L. extract
PBS	phosphate-buffered saline
PE	polyethylene
ROS	reactive oxygen species
SEM	scanning electron microscopy
ZDTC	zinc diethyldithiocarbamate

■ REFERENCES

(1) Liang, Y.; Liang, Y.; Zhang, H.; Guo, B. Antibacterial biomaterials for skin wound dressing. *AJPS* **2022**, *17*, 353−384.

(2) Gao, C.; Zhang, L.; Wang, J.; Jin, M.; Tang, Q.; Chen, Z.; Cheng, Y.; Yang, R.; Zhao, G. Electrospun Nanofibers Promote Wound Healing: Theories, Techniques and Perspectives. *J. Mater. Chem. B* **2021**, *9* (14), 3106−3130.

(3) Li, L.; Hao, R.; Qin, J.; Song, J.; Chen, X.; Rao, F.; Zhai, J.; Zhao, Y.; Zhang, L.; Xue, J. Electrospun Fibers Control Drug Delivery for Tissue Regeneration and Cancer Therapy. *Adv. Fiber Mater.* **2022**, *4*, 1375−1413.

(4) Li, Z.; Mei, S.; Dong, Y.; She, M.; Li, Y.; Li, P.; Kong, L. Functional Nanofibrous Biomaterials of Tailored Structures for Drug Delivery—A Critical Review. *Pharmaceutics* **2020**, *12* (6), 522−545.

(5) (a) Ali, I.; Ouf, A.; Elshishiny, F.; Taskin, M.; Song, J.; Dong, M.; Chen, M.; Siam, R.; Mamdouh, W. Antimicrobial and Wound-Healing Activities of Graphene-Reinforced Electrospun Chitosan/Gelatin Nanofibrous Nanocomposite Scaffolds. *ACS Omega* **2022**, *7* (2), 1838−1850. (b) Hamdi, M.; Elkashlan, A.; Hammad, M.; Ali, I. SARS-CoV-2 Papain-like Protease Responsive ZnO/Daclatasvir-Loaded Chitosan/Gelatin Nanofibers as Smart Antimicrobial Medical Textiles: In Silico, In Vitro and Cell Studies. *Pharmaceutics* **2023**, *15* (8), 2074−2099. (c) Wang, H.; Ding, F.; Ma, L.; Zhang, Y. Edible films from chitosan-gelatin: Physical properties and food packaging application. *Food Biosci* **2021**, *40*, 100871−100888.

(6) Ahmadi, S.; Hivechi, A.; Bahrami, H.; Milan, P.; Ashraf, S. Cinnamon extract loaded electrospun chitosan/gelatin membrane with antibacterial activity. *Int. J. Biol. Macromol.* **2021**, *173*, 580−590.

(7) Vo, T. S.; Vo, T. T. B. C.; Vo, T. T. T. N.; Lai, T. N. H. Turmeric, L., Curcuma longa, L. Turmeric (Curcuma longa L.): Chemical Components and Their Effective Clinical Application-sChemical Components and Their Effective Clinical Applications. *J. Turkish chem. soc* **2021**, *8*, 883−898.

(8) Alqaseer, K.; Idreess, H. G.; Saed, E.; Radhi, O.; Shnain, W.; Falah, M.; Al-Roubaey, D.; Sarhan, N. H.; Ali, A.; Hashem, F. Turmeric: An important medicinal plant in the treatment of many diseases: A review Study. *KJNS* **2023**, *13* (2), 229−237.

(9) Rasouli, S.; Montazeri, M.; Mashayekhi, S.; Sadeghi-Soureh, S.; Dadashpour, M.; Mousazadeh, H.; Nobakht, A.; Zarghami, N.; Pilehvar-Soltanahmadi, Y. Synergistic anticancer effects of electrospun nanofiber-mediated codelivery of Curcumin and Chrysin: Possible application in prevention of breast cancer local recurrence. *J. Drug Delivery Technol.* **2020**, *55*, 101402.

(10) Li, Y.; Ertas, Y.; Jafari, A.; Taheri, M.; Pilehvar, Y. Co-delivery of curcumin and chrysin through pH-sensitive hyaluronan-modified hollow mesoporous silica nanoparticles for enhanced synergistic anticancer efficiency against thyroid cancer cells. *J. Drug Delivery Technol.* **2023**, *87*, 104787.

(11) Mohammadi, Z.; Sharif-zak, M.; Majdi, H.; Mostafavi, E.; Barati, M.; Lotfimehr, H.; Ghaseminasab, K.; Pazoki-Toroudi, H.; Webster, T.; Akbarzadeh, A. The effect of chrysin−curcumin-loaded nanofibres on the wound-healing process in male rats. *Artif. Cells, Nanomed., Biotechnol.* **2019**, *47* (1), 1642−1652.

(12) Stompor-Gorący, M.; Bajek-Bil, A.; Machaczka, M. Chrysin: Perspectives on Contemporary Status and Future Possibilities as Pro-Health Agent. *Nutrients* **2021**, *13* (6), 2038−2055.

(13) Alipour, M.; Pouya, B.; Aghazadeh, Z.; SamadiKafil, H.; Ghorbani, M.; Alizadeh, S.; Aghazadeh, M.; Dalir Abdolahinia, E. The Antimicrobial, Antioxidative, and Anti-Inflammatory Effects of Polycaprolactone/Gelatin Scaffolds Containing Chrysin for Regenerative Endodontic Purposes. *Stem Cells Int.* **2021**, *2021*, 1−11.

(14) Alven, S.; Nqoro, X.; Aderibigbe, B. Polymer-Based Materials Loaded with Curcumin for Wound Healing Applications. *Polym.* **2020**, *12*, 2286.

(15) Gaydhane, M.; Sharma, C.; Majumdar, S. Electrospun nanofibres in drug delivery: advances in controlled release strategies. *RSC Adv.* **2023**, *13*, 7312−7328.

(16) Lawson, H.; Walton, S.; Chan, C. Metal−Organic Frameworks for Drug Delivery: A Design Perspective. *ACS Appl. Mater. Interfaces* **2021**, *13* (6), 7004−7020.

(17) Yang, J.; Yang, Y.-W. Metal−Organic Frameworks for Biomedical Applications. *Small* **2020**, *16*, 1906846−1906870.

https://doi.org/10.1021/acsomega.4c08100
ACS Omega 2025, 10, 21065−21076

(18) Yang, L.; Wang, K.; Guo, L.; Hu, X.; Zhou, M. Unveiling the potential of HKUST-1: synthesis, activation, advantages and biomedical applications. *J. Mater. Chem. B* **2024**, *12*, 2670−2690.
(19) Wang, Y.; Kang, H.; Hu, J.; Chen, H.; Zhou, H.; Wang, Y.; Ke, H. Preparation of metal-organic framework combined with Portulaca oleracea L. extract electrostatically spun nanofiber membranes delayed release wound dressing. *RSC Adv.* **2023**, *13*, 21633−21642.
(20) Mohammadnejad, M.; Fakhrefatemi, M. Synthesis of magnetic HKUST-1 metal-organic framework for efficient removal of mefenamic acid from water. *J. Mol. Struct.* **2021**, *1224*, 129041−129048.
(21) Zhang, P.; Li, Y.; Tang, Y.; Shen, H.; Li, J.; Yi, Z.; Ke, Q.; Xu, H. Copper-Based Metal-Organic Framework as A Controllable Nitric Oxide-Releasing Vehicle for Enhanced Diabetic Wound Healing. *ACS Appl. Mater. Interfaces* **2020**, *12* (16), 18319−18331.
(22) Lawson, S.; Newport, K.; Pederniera, N.; Rownaghi, A.; Rezaei, F. Curcumin Delivery on Metal−Organic Frameworks: The Effect of the Metal Center on Pharmacokinetics within the M-MOF-74 Family. *ACS Appl. Bio Mater.* **2021**, *4* (4), 3423−3432.
(23) Zhang, Z.-J.; Hou, Y.-K.; Chen, M.-W.; Yu, X.-Z.; Chen, S.-Y.; Yue, Y.-R.; Guo, X.-T.; Chen, J.-X.; Zhou, Q. A pH-responsive metal-organic framework for the co-delivery of HIF-2α siRNA and curcumin for enhanced therapy of osteoarthritis. *J. Nanobiotechnology* **2023**, *21*, 1−19.
(24) Santadkha, T.; Skolpap, W.; Thitapakorn, V. Diffusion Modeling and In Vitro Release Kinetics Studies of Curcumin−Loaded Superparamagnetic Nanomicelles in Cancer Drug Delivery System. *J. Pharm. Sci.* **2022**, *111* (6), 1690−1699.
(25) Ting, P.; Srinuanchai, W.; Suttisansanee, U.; Tuntipopipat, S.; Charoenkiatkul, S.; Praengam, K.; Chantong, B.; Temviriyanukul, P.; Nuchuchua, O. Development of Chrysin Loaded Oil-in-Water Nanoemulsion for Improving Bioaccessibility. *Foods* **2021**, *10*, 1912.
(26) Suryati, S.; Meriatna, M.; Sulhatun, St.; Dwi, A. Lestari. Preparation and Characterization of Chitosan-Gelatin-Glycerol Biocomposite for Primary Wound Dressing. *Int. J. Eng.* **2022**, *2* (1), 64−69.
(27) Hajzamani, D.; Shokrollahi, P.; Najmoddin, N.; Shokrolahi, F. Effect of engineered PLGA-gelatin-chitosan/PLGA-gelatin/PLGA-gelatin-graphene three-layer scaffold on adhesion/proliferation of HUVECs. *Polym. Adv. Technol.* **2020**, *31* (9), 1896−1910.
(28) Alizadeh, N.; Malakzadeh, S. Antioxidant, antibacterial and anti-cancer activities of β-and γ-CDs/curcumin loaded in chitosan nanoparticles. *Int. J. Biol. Macromol.* **2020**, *147*, 778−791.
(29) Jangid, A.; Solanki, R.; Patel, S.; Medicherla, K.; Pooja, D.; Kulhari, H. Improving Anticancer Activity of Chrysin using Tumor Microenvironment pH-Responsive and Self-Assembled Nanoparticles. *ACS Omega* **2022**, *7* (18), 15919−15928.
(30) Shamloo, A.; Aghababaie, Z.; Afjoul, H.; Jami, M.; Bidgoli, M. R.; Vossoughi, M.; Ramazani, A.; kamyabhesari, k. Fabrication and evaluation of chitosan/gelatin/PVA hydrogel incorporating honey for wound healing applications: An in vitro, in vivo study. *Int. J. Pharm.* **2021**, *592*, 120068.
(31) Sreekantan, S.; Hassan, M.; Sundera Murthe, S.; Seeni, A. Biocompatibility and Cytotoxicity Study of Polydimethylsiloxane (PDMS) and Palm Oil Fuel Ash (POFA) Sustainable Super-Hydrophobic Coating for Biomedical Applications. *Polymers* **2020**, *12* (12), 3034−3047.
(32) Boroumand, S.; Majidi, R.; Gheibi, A.; Majidi, R. Selenium nanoparticles incorporated in nanofibers media eliminate H1N1 activity: a novel approach for virucidal antiviral and antibacterial respiratory mask. *ESPR* **2024**, *31*, 2360−2376.
(33) Nabipour, H.; Aliakbari, F.; Volkening, K.; Strong, M.; Rohani, S. New metal-organic framework coated sodium alginate for the delivery of curcumin as a sustainable drug delivery and cancer therapy system. *Int. J. Biol. Macromol.* **2024**, *259*, 128875−1288887.
(34) Drosou, C.; Krokida, M.; Biliaderis, C. G. Encapsulation of β-carotene into food-grade nanofibers via coaxial electrospinning of hydrocolloids: Enhancement of oxidative stability and photo-protection. *Food Hydrocolloids* **2022**, *133*, 107949−107966.
(35) (a) Yousefian, M.; Rafiee, Z. Cu-metal-organic framework supported on chitosan for efficient condensation of aromatic aldehydes and malononitrile. *Carbohydr. Polym.* **2020**, *228*, 115393−115401. (b) Yu, H.; Wu, H.; Tian, X.; Zhou, Y.; Ren, C.; Wang, Z. A nano-sized Cu-MOF with high peroxidase-like activity and its potential application in colorimetric detection of H 2 O 2 and glucose. *RSC Adv.* **2021**, *11*, 26963−26973. (c) Insan, D.; Rekhi, H.; Kaur, H.; Singh, K.; Malik, A. A Novel Method for the Synthesis of MOF-199 for Sensing and Photocatalytic Applications. *J. Fluoresc.* **2022**, *32*, 1171−1188.
(36) (a) Sakthiguru, N.; Sithique, M. Fabrication of bioinspired chitosan/gelatin/allantoin biocomposite film for wound dressing application. *Int. J. Biol. Macromol.* **2020**, *152*, 873−883. (b) Liu, F.; Liu, Y.; Sun, Z.; Wang, D.; Wu, H.; Du, L.; Wang, D. Preparation and antibacterial properties of ε-polylysine-containing gelatin/chitosan nanofiber films. *Int. J. Biol. Macromol.* **2020**, *164*, 3376−3387.
(37) (a) Suteris, N.; Yasin, A.; Misnon, I. I.; Roslan, R.; Zulkifli, F.; Rahim, M. H. A.; Venugopal, J.; Jose, R. Curcumin loaded waste biomass resourced cellulosic nanofiber cloth as a potential scaffold for regenerative medicine: An in-vitro assessment. *Int. J. Biol. Macromol.* **2022**, *198*, 147−156. (b) Khasteband, M.; Sharifi, Y.; Akbari, A. Chrysin loaded polycaprolactone-chitosan electrospun nanofibers as potential antimicrobial wound dressing. *Int. J. Biol. Macromol.* **2024**, *263*, 130250−130259.
(38) Liang, Y.; Yao, Y.; Liu, Y.; Li, Y.; Xu, C.; Fu, L.; Lin, B. Curcumin-loaded HKUST-1@ carboxymethyl starch-based composites with moisture-responsive release properties and synergistic antibacterial effect for perishable fruits. *Int. J. Biol. Macromol.* **2022**, *214*, 181−191.
(39) Xu, L.; Liu, Y.; Zhou, W.; Yu, D. Electrospun Medical Sutures for Wound Healing: A Review. *Polym.* **2022**, *14* (9), 1637−1666.
(40) Lanno, G.-M.; Ramos, C.; Preem, L.; Putrinš, M.; Laidmäe, I.; Tenson, T.; Kogermann, K. Antibacterial Porous Electrospun Fibers as Skin Scaffolds for Wound Healing Applications. *ACS Omega* **2020**, *5*, 30011−30022.
(41) Snetkov, P.; Rogacheva, E.; Kremleva, A.; Morozkina, S.; Uspenskaya, M.; Kraeva, L. In-Vitro Antibacterial Activity of Curcumin-Loaded Nanofibers Based on Hyaluronic Acid against Multidrug-Resistant ESKAPE Pathogens. *Pharmaceutics* **2022**, *14* (6), 1186−1206.
(42) Duan, M.; Sun, J.; Huang, Y.; Jiang, H.; Hu, Y.; Pang, J.; Wu, C. Electrospun gelatin/chitosan nanofibers containing curcumin for multifunctional food packaging. *Food Sci. Hum. Wellness* **2023**, *12*, 614−621.
(43) Mahmud, M. M.; Zaman, S.; Perveen, A.; Jahan, R.; Islam, M.; Arafat, M. T. Controlled release of curcumin from electrospun fiber mats with antibacterial activity. *J. Drug Deliv Sci. Technol.* **2020**, *55*, 101386−101395.
(44) Wu, X. Q.; Mirza, N.; Huang, Z.; Zhang, J.; Zheng, Y.-M.; Xiang, J.; Xie, Z. Enhanced desalination performance of aluminium fumarate MOF-incorporated electrospun nanofiber membrane with bead-on-string structure for membrane distillation. *Desalination* **2021**, *520*, 115338.
(45) Sun, Y.; Zheng, L.; Yang, Y.; Qian, X.; Fu, T.; Li, X.; Yang, Z.; Yan, H.; Cui, C.; Tan, W. Metal−Organic Framework Nanocarriers for Drug Delivery in Biomedical Applications. *Nanomicro Lett.* **2020**, *12*, 103−132.
(46) Dong, X.; Cao, Y.; Wang, N.; Wang, P.; Li, M. Systematic study on solubility of chrysin in different organic solvents: The synergistic effect of multiple intermolecular interactions on the dissolution process. *J. Mol. Liq.* **2021**, *325*, 115180.
(47) (a) Sharma, A.; Mittal, A.; Puri, V.; Kumar, P.; Singh, I. Curcumin-loaded, alginate−gelatin composite fibers for wound healing applications. *3 Biotech* **2020**, *10*, 464. (b) Zahiri, M.; Khanmohammadi, M.; Goodarzi, A.; Ababzadeh, S.; Sagharjoghi Farahani, M.; Mohandesnezhad, S.; Bahrami, N.; Nabipour, I.; Ai, J. Encapsulation of curcumin loaded chitosan nanoparticle within poly (ε-caprolactone) and gelatin fiber mat for wound healing and layered dermal reconstitution. *Int. J. Biol. Macromol.* **2020**, *153*, 1241−1250.

https://doi.org/10.1021/acsomega.4c08100
ACS Omega 2025, 10, 21065−21076

(c) Sadeghi-Soureh, S.; Jafari, R.; Gholikhani-Darbroud, R.; Pilehvar-Soltanahmadi, Y. Potential of Chrysin-loaded PCL/gelatin nanofibers for modulation of macrophage functional polarity towards anti-inflammatory/pro-regenerative phenotype. *J. Drug Delivery Technol.* **2020**, *58*, 101802.
(48) Fahimirad, S.; Abtahi, H.; Satei, P.; Ghaznavi-Rad, E.; Moslehi, M.; Ganji, A. Wound healing performance of PCL/Chitosan based electrospun nanofiber electrosprayed with curcumin loaded chitosan nanoparticles. *Carbohydr. Polym.* **2021**, *259*, 117640−117653.
(49) Shetty, K.; Bhandari, A.; Yadav, K. Nanoparticles incorporated in nanofibers using electrospinning: A novel nano-in-nano delivery system. *JCR* **2022**, *350*, 421−434.
(50) Ekawati, E.; Darmanto, W.; Wahyuningsih, s. p. a. Detection of Staphylococcus aureus in wound infection on the skin surface. *IOP Conference Series: Earth and Environmental Science* 2020, *456*, 012038..
(51) Phan, S.; Feng, C.; Huang, R.; Lee, Z.; Moua, Y.; Phung, O.; Lenhard, J. Relative Abundance and Detection of Pseudomonas aeruginosa from Chronic Wound Infections Globally. *Microorganisms* **2023**, *11*, 1210−1224.
(52) Kaur, N.; Tiwari, P.; Kapoor, K.; Saini, A.; Sharma, V.; Mobin, S. Metal-organic framework based antibiotic release and antimicrobial response: An overview. *CrystEngComm* **2020**, *22*, 7513−7527.
(53) Fahimirad, S.; Fahimirad, Z.; Sillanpää, M. Efficient removal of water bacteria and viruses using electrospun nanofibers. *Sci. Total Environ.* **2021**, *751*, 141673−141691.

https://doi.org/10.1021/acsomega.4c08100
ACS Omega 2025, 10, 21065−21076